Effect of lubricant rheology on hypoid gear pair efficiency

3rd Biennial International Conference on Powertrain Modelling and Control (PMC 2016)
Testing, Mapping and Calibration
7th-9th September 2016, Loughborough University, UK

Effect of Lubricant Rheology on Hypoid Gear Pair Efficiency

L. Paouris [1*], S. Theodossiades [1], R. Rahmani [1], H. Rahnejat [1], G. Hunt [2], W. Barton [2]

[1] Wolfson School of Mechanical, Electrical and Manufacturing Engineering, Loughborough University, Loughborough, Leicestershire, UK

[2] Applied Sciences Department, Lubrizol Ltd., Hazelwood, Derby, Derbyshire, UK

[*] Corresponding author: L.Paouris@lboro.ac.uk

Abstract

A tribo-dynamics model of a differential hypoid gear pair is presented, integrated with lubricated contact of meshing teeth pair with lubricants of varying rheological properties. Particular attention is paid to the effect of lubricant formulation and gear geometry on the system efficiency. The influence of gear torsional dynamic response is taken into account in a 4-Degree of Freedom (DoF) model. The contact geometry and kinematics of the hypoid gear pair are estimated, using Tooth Contact Analysis (TCA). Two fully formulated gear lubricants of the same viscosity grade (SAE 75W-90) blended with the same additive pack, but with different types and concentration of viscosity modifier (VM) are considered. Conjunctional friction is predicted for viscous shear of fully characterised lubricants as well as boundary interaction of rough surfaces. The results show loss of friction resulting in resonant response of the gear pair with impact of meshing teeth exhibiting non-linear jump phenomenon. The predictions also show that lubricants with higher pressure – viscosity (PV) coefficients tend to exhibit increased power loss.

Keywords: *Hypoid Gear pair, Elastohydrodynamics, Gear Dynamics, Friction, Jump phenomenon, Resonance, Lubricant Rheology*

1-Introduction

The hypoid gear pair is a major power transmitting system used in the differential units of trucks, vans modern passenger cars. Its function is to transmit the power provided by the engine through the main driveshaft to the axle half-shafts, connected to the driven wheels. Due to its position within the powertrain and its special geometrical features, the differential frequently operates under high loads and sliding velocities, applied to their teeth pairs in

mesh. Thus, the system is subjected to appreciable frictional power loss. The trends in automotive industry is focused on fuel efficiency and low emissions designs, thus design of power transmitting components such as hypoid gearing is increasingly subject to detailed design analysis [1, 2].

There is a dearth of predictive analysis for hypoid gears relative to other form of gearing systems. Kubo et al [3] examined the effect of the lubricant viscosity grade and type of the friction modifier on the transmission efficiency of a typical vehicle drivetrain unit. A rear axle configuration was used and the experimental setup allowed measurement of power losses in the rear axle, comprising the differential hypoid gears. The results of this analysis indicated that the use of transmission fluids with reduced viscosity improved the efficiency of the rear axle at lower temperatures, although for higher temperatures this deteriorated, possibly due to the effect of teeth surface asperity interactions. The use of multi-grade oils was recommended as a counter measure. Despite the solid evidence of an experimental study, this study did not lead in isolation of the contribution of conjunctional power losses on the total efficiency of the rear axle, since this are other contributions due to contamination, as well as churning and bearing losses. Xu and Kahraman [4] developed a hypoid gear pair friction model which was able to calculate the conjunctional power losses of such gears. The trends of their results were in good general agreement with measurements of Kubo et al [3]. Karagiannis et al [5] as well as Mohammadpour et al [1,6,7] examined theoretically the lubrication of automotive differential hypoid gears under dynamic conditions. Their findings included the impact of the gear dynamics on the conjunctional power losses of the system, particularly for operating conditions near the resonant frequency where vibro-impact phenomena appear (single/double sided tooth impacts). The non-Newtonian tractive nature of teeth pair conjunctions was also demonstrated as well as the effect of inlet starvation [7]. They also noted the often contrary requirements between noise and vibration performance and transmission efficiency [6]. Recently, Talbot et al [8] presented a friction model, capable of predicting the conjunctional losses, the bearing losses and the churning losses in an automotive rear axle. Very good agreement with experimental measurement was demonstrated.

There remains a gap in the open literature with regard to the influence of lubricant formulation on the conjunctional efficiency of hypoid gear pairs. In this paper particular attention is paid to the characterisation of lubricant viscosity in high shear, highs pressure and temperature, which are commonly encountered in hypoid gear pairs. The effect of several

lubricant-related viscosity parameters on the power losses is examined, highlighting the influence of the high pressure behaviour of the fluid and enabling the design of more fuel efficient gear lubricants. Furthermore, the effect of gear ratio on the system efficiency is investigated, suggesting that gear pairs with lower gear ratios exhibit improved efficiency characteristics under the same operating conditions.

2-Theory and Governing Equations

In order to predict efficiency of hypoid gear pairs the problem is decomposed into three subset problems, which are treated separately: (1) Tooth Contact Analysis (TCA), (2) development of a friction model and (3) development of a torsional gear dynamics model. TCA is performed in order to obtain contact geometry and kinematics of meshing teeth pairs. It is based on a quasi-static contact Finite Element (FE) analysis of the gear pair under investigation. TCA is performed using CALYX (Vijayakar [9]). In order to do so, the geometry of the hypoid gear pair needs to be described. The information describing the geometry and the assembly of a hypoid gear pair are contained in a file usually known as the Special Analysis File (SPA), which is then used in TCA. The SPA is provided by the gear manufacturer and it contains all the information required to create the solid model of the hypoid gear pair under investigation. The friction model is used to predict friction between the contacting flanks at each time step of time in the meshing cycle, assuming that the prevailing regime of lubrication is Elastohydrodynamic (EHD) (also referred to as piezo viscous – elastic). The high pressure, high shear rate and high temperature responses of the lubricant under investigation are essential inputs at this stage, because they can directly affect the lubricant film thickness, and thus the generated friction. Finally, the torsional gear dynamics model, coupled with friction would enable prediction of torsional oscillations, thus vibration performance of the system as a whole in the same manner as in [6].

2.1-Tooth contact analysis (TCA)

In terms of their geometry, hypoid gear pairs can be considered as the most general case of gearing, meaning that any other type of gearing (such as a spur or a bevel gear pair) can be represented as a simplified form of a hypoid gear pair [7]. Therefore, hypoid gears exhibit a rather complex tooth geometry, which is reflected in their geometry and the kinematics of contact. In order to perform a successful tribological and gear dynamics analyses, contact-related parameters need to be known a priori. However, the rather complex teeth geometry

does not lend itself to simple analytical deduction of these parameters. Consequently, these are calculated through numerical techniques. TCA is used for this purpose. As it can be seen in Fig. 1a, b solid finite element model of the hypoid gear pair can be created, when a full set of geometrical parameters is available, usually through the SPA provided by the gear manufacturer. For the purposes of the present study, three gear sets are examined, with some of their geometrical characteristics listed in table 1.

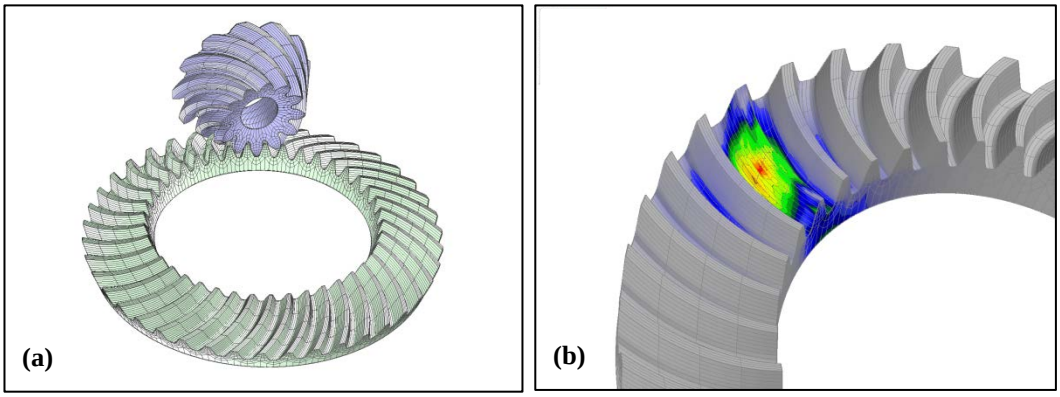

Figure 1: (a) FE model of a typical gear-set and (b) the corresponding Von Mises stress distribution

The parameters listed in table 1, along with a plethora of others, are used in TCA to create a solid model of the hypoid gear pair, which is then discretised using solid elements (Fig. 1). Gear-set 1 is used as the baseline model to demonstrate the tribological performance of the system under different operating conditions (speed, load) and with the influence of different lubricant formulations. Gear-sets 2 and 3 are of very similar geometry, with the main difference being the gear ratio (2.73 for gear-set 2 and 3.41 for gear-set 3). Gear-sets 2 and 3 are used to demonstrate the effect of gear ratio on the conjunctional efficiency. All the three gear sets are face-hobbed.

Once TCA is completed for a given combination of pinion speed and input torque, outputs such as the von Mises stress distribution in the contact zone (Fig. 1b), as well as the point and the path of the contact between the mating teeth are determined. The parameters of interest, ought through TCA are: (1) the principal contact radii of the pinion and ring gear contacting teeth at any meshing location, (2) the unloaded static transmission error, (3) the meshing stiffness and its variation with applied load, (4) the load share per teeth pair contact, (5) the radii of curvature of the mating teeth at the point of contact along the semi-minor and the semi-major axes of the elliptical contact footprint, and (6) the instantaneous surface velocities

of the teeth along these principal axes. All the aforementioned quantities vary periodically with the pinion angle of rotation. The methodology followed to determine each of these parameters is described by Karagiannis at al [5].

Table 1: Main geometrical parameters of the examined gear-sets

Parameter (unit)	Gear-set 1		Gear-set 2		Gear-set 3	
	Pinion	Ring	Pinion	Ring	Pinion	Ring
Number of teeth (−)	13	36	15	41	12	41
Face width (**mm**)	33.85	30	40.76	38.20	39.38	36.50
Face angle (°)	29.05	59.65	27.77	61.60	22.74	66.70
Spiral angle (°)	46	27.60	40	26.96	40	26.62
Outer cone distance (**mm**)	83.08	95.60	95.63	112.53	92.42	107.80
Offset (**mm**)	24	24	20	20	20	20

Fig. 2 illustrates the variation of meshing stiffness with the pinion rotation angle for the gear-set 3 and for 3 different input torque values. Its mean value and the peak-to-peak variations vary with the input torque. This is also observed in the analysis of Karagiannis et al [10].

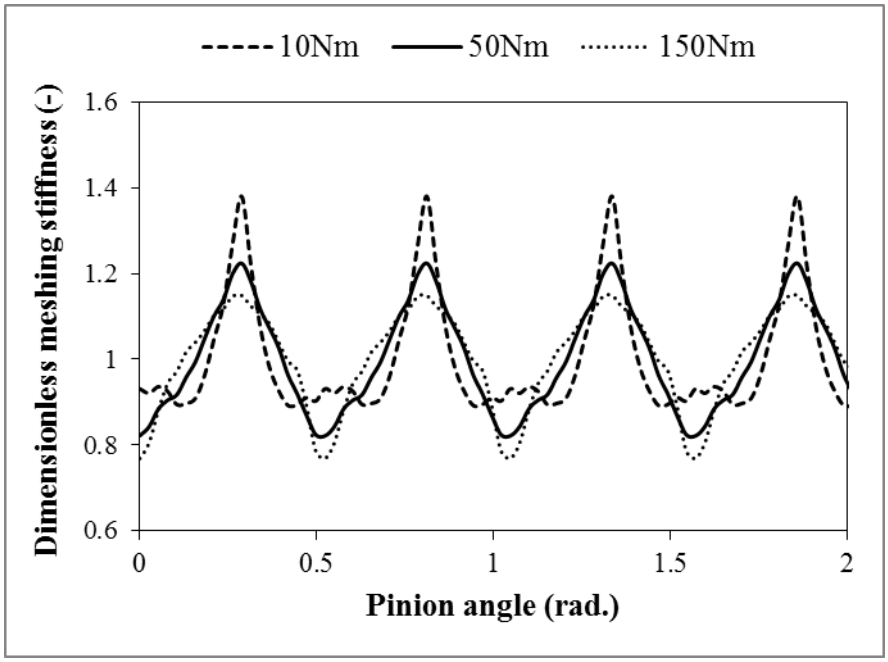

Figure 2: Variation of dimensionless meshing stiffness with pinion angle for the gear-set 3

In order to account for the variation of the gear teeth meshing data, the TCA-determined teeth contact parameters with respect to the pinion angle are fitted with a Fourier series as:

$$R_p = R_{p,0} + \sum_{i=1}^{8} R_{ps,i}\sin\left(iN_p\varphi_p\right) + \sum_{i=1}^{8} R_{pc,i}\cos\left(iN_p\varphi_p\right) \qquad (1)$$

$$e_0 = e_{0,0} + \sum_{i=1}^{8} e_{ps,i}\sin\left(iN_p\varphi_p\right) + \sum_{i=1}^{8} e_{ps,i}\sin\left(iN_p\varphi_p\right) \qquad (2)$$

$$k_m = k_{m,0} + \sum_{i=1}^{8} k_{ps,i}\sin\left(iN_p\varphi_p\right) + \sum_{i=1}^{8} k_{ps,i}\sin\left(iN_p\varphi_p\right) \qquad (3)$$

$$lf_k = lf_0 + \sum_{i=1}^{8} lf_{ps,i}\sin\left(\frac{1}{3}iN_p\varphi_p\right) + \sum_{i=1}^{8} lf_{ps,i}\sin\left(\frac{1}{3}iN_p\varphi_p\right) \qquad (4)$$

The argument of the trigonometric functions in equations (1) – (3) is: $N_p\varphi_p = N_p\omega_p t = \omega_m t$, where ω_m is the meshing angular frequency, which is related to the meshing period T_m. Equations (1) – (3) assume that the contact load is the sum of the individual flank loads. This is applied at a single point. This assumption is accurate for the description of the torsional gear dynamics of the system [11]. For a tribological study contact kinematics and load carried by a pair of teeth, rather than the total contact load need to be known. Equation (4) describes the load sharing factor for 2-3 simultaneous teeth pairs in contact. The load share factor is defined as the ratio of the individual flank contact load over the total contact load carried by the gear pair at a any instant of time, hence: $lf_k = W_k/W_t = lf_k\left(\varphi_p\right)$ $(W_t = W_1 + W_2 + W_3)$.

2.2-Friction model

Flank friction is calculated using an analytical model, assuming that the prevailing regime of lubrication is piezo-viscous – elastic (i.e. hard EHD). Both the viscous and boundary components of friction are accounted for in the calculation process, thus:

$$F_{fr} = F_v + F_b \qquad (5)$$

where, F_v is the contribution due to viscous friction, while F_b is that due to asperity (or boundary) friction. The viscous component is:

$$F_v = \left(A_{EHL} - A_{asp}\right)\overline{\tau} \quad (6)$$

where, $A_{EHL} = \pi a_c b_c$ is the area of the elliptical contact footprint between the mating flanks and A_{asp} is the predicted area of asperity. The semi-major and the semi-minor axes of the contact footprint ($a_c$and b_c) are calculated according to Hamrock and Dowson [12]. Finally, $\overline{\tau}$ is the average viscous shear stress:

$$\overline{\tau} = \frac{\eta\left(p, \overline{T}_c\right)}{F(\dot{\gamma})}\dot{\gamma} \quad (7)$$

where, $\eta\left(p, \overline{T}_c\right)$ is the low shear dynamic viscosity of the lubricant at pressure p and temperature $\overline{T}_c$, is the average temperature at the centre of the conjunction. Roelands equation [13] is used to describe the variation viscosity with pressure and Vogel's for the variation of the same with temperature [14]. The parameter $F(\dot{\gamma})$ is used to describe the shear thinning of the lubricant at higher shear rates (non – Newtonian response) and for the lubricants examined this is calculated according to the Havriliak – Negami model [15] as:

$$F(\dot{\gamma}) = (1 + (\lambda\dot{\gamma})^{\alpha_{HN}})^{\beta_{HN}} \quad (8)$$

In equation (8), λ is the relaxation time of the polymeric solution, while α_{HN} and β_{HN} are related to the distribution of the molecular weight of the blended polymers and the structure of the polymer chains. The high shear response of the viscosity is determined at ambient pressure and at 70 ℃, using an ultra-high shear viscometer (USV).

Table 2: Lubricant properties

Parameter (unit)	**OS265962**	**OS265963**
$\boldsymbol{\lambda}$ **(s)**	7.9×10^{-8}	8.0×10^{-8}
$\boldsymbol{\alpha_{HN}}$ $(-)$	0.70	0.97
$\boldsymbol{\beta_{HN}}$ $(-)$	1	1
$\boldsymbol{\alpha^*}$ **at 40 ℃** $(\mathbf{GPa^{-1}})$	16.09	19.31
$\boldsymbol{\alpha^*}$ **at 100 ℃** $(\mathbf{GPa^{-1}})$	11.59	13.89
$\boldsymbol{\alpha^*}$ **at 140 ℃** $(\mathbf{GPa^{-1}})$	9.38	12.28
$\boldsymbol{k_f}$ $(\mathbf{W/m.K})$	0.18	0.80
$\boldsymbol{c_{p,f}}$ $(\mathbf{J/kg.K})$	2090	2090

The high pressure viscosity is measured for pressures up to 0.5 GPa through a high pressure falling body viscometer at three different temperatures(40 ℃, 100 ℃ and 140 ℃), yielding the corresponding pressure viscosity coefficient; α^*. All the viscosity related data are provided by the lubricant manufacturer. Table 2 lists the lubricant rheological parameters used in the current analysis.

A comparison of the lubricant parameters in table 2 shows that the fluids under examination have different high shear and high pressure responses. The effect of those differences is investigated in the current study. Finally, the viscous shear rate $\dot{\gamma}$ is calculated as:

$$\dot{\gamma} = \frac{|V_s|}{h_c} \quad (9)$$

where, V_s is the sliding speed between the mating flank surfaces and h_c is the central lubricant film thickness [16]:

$$h_c = 4.31 R_e {U_e}^{0.68} G^{0.49} {W_e}^{-0.073} \left[1 - \exp\left(-1.23 (R_s/R_e)^{2/3}\right)\right] \quad (10)$$

The parameters in equation (10) depend on the operating conditions (lubricant entraining velocity, contact load, etc.) and the lubricant properties (low shear dynamic viscosity and the PV coefficient) and are calculated according to those stated by Chittenden et al [16].

The boundary friction force is calculated according to as [17]

$$F_b = \tau_0 A_{asp} + \varsigma_a W_{asp} \quad (11)$$

Eyring shear stress is $\tau_0 \approx 2$ MPa for most lubricant, indicating the onset of non-Newtonian behaviour of thin adsorbed boundary films [18], $\varsigma_a = 0.17$ is analogous to the coefficient of friction (i.e. coefficient of shear strength of asperities on the softer of the two counter faces) [17]. This is usually measured using atomic force microscopy, operating in lateral force mode as shown by Styles et al [19] and Leighton et al [20]. W_{asp} is the share of contact load carried by the asperities. Quantities A_{asp} and W_{asp} are calculated according to Greenwood and Tripp [21], assuming a Gaussian distribution of asperity heights:

$$W_{asp} = \frac{8\sqrt{2}}{15} \pi A_{EHL} \left(\eta_s \beta_s \sigma_{s,c}\right)^2 \sqrt{\frac{\sigma_s}{\beta_s}} E^* F_{5/2} \quad (12)$$

$$A_{asp} = \pi^2 A_{EHL}\left(\eta_s \beta_s \sigma_{s,c}\right)^2 F_2 \qquad (13)$$

In equations (12) and (13) require the statistical functions $F_{5/2}$ and F_2, which depend on the Stribeck lubricant film ratio $\lambda_s = h_c/\sigma_{s,c}$ ($\sigma_{s,c} = \sqrt{2}\sigma_s$ for Gaussian surfaces having the same surface height distribution). The parameters η_s, β_s and σ_s correspond to the density of the asperity peaks per unit area, the average radius of curvature of the asperity tips and their root mean square (RMS) height above the mean line respectively. The magnitude of each one of those parameters has been determined through measuring the surface height distribution of a run-in hypoid pinion pair using an infinite focus white light interferometer; Alicona with vertical measurement resolution of 1 nm and horizontal resolution of 175 nm. Fig. 3 illustrates a 2D contour plot of the surface height distribution for a run-in hypoid pinion tooth.

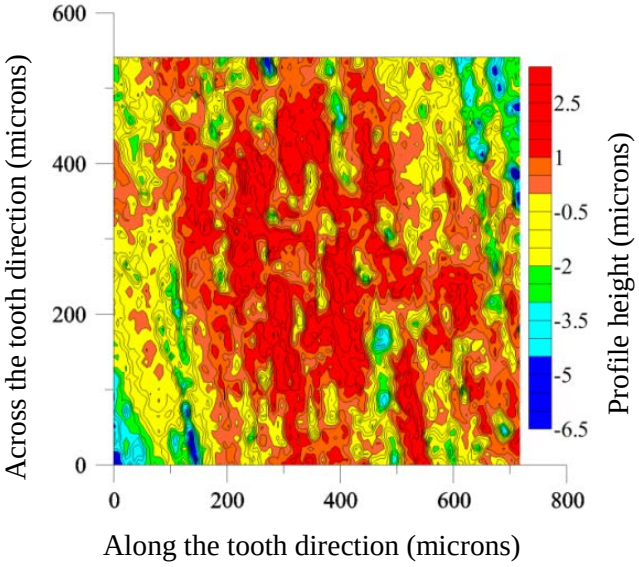

Figure 3: 2-dimensional contour plot of the surface asperity height distribution

The post-processing of the surface height measurements (Fig. 3) yields the aforementioned surface topographical parameters. $\eta_s \beta_s \sigma_{s,c}$ is known as the surface roughness parameter and the ratio $\frac{\sigma_s}{\beta_s}$ is a measure of the asperity slope (sharpness) [22]. For the run-in pinion tooth: $\eta_s \beta_s \sigma_{s,c} = 0.0104$ which is lower than the minimum range suggested by Greenwood and Tripp [21], indicating high polishing of the pinion flank during the running-in process.

Finally, an analytical thermal model is employed to estimate the temperature rise of the lubricant at the centre of the conjunction due to frictional heating. The average temperature at the centre of the conjunction can be calculated as:

$$\overline{T}_c = T_{in} + \left(\Delta T_f\right)_{av} + (\Delta T_{oil})_{av} \quad (14)$$

where, the inlet temperature is found as:

$$T_{in} = T_{bath} + 20\,℃ \quad (15)$$

The $20\,℃$ increase in the inlet temperature is an approximate value, valid for a wide combination of speeds and loads, according to Olver [23]. The average flash temperature rise $\left(\Delta T_f\right)_{av}$ and the average temperature rise of the lubricant due to shear heating $(\Delta T_{oil})_{av}$ are calculated as [23, 24]:

$$\left(\Delta T_f\right)_{av} = R_{f,p} a_h \dot{q} \quad \text{and} \quad (\Delta T_{oil})_{av} = \frac{|V_s|\overline{\tau} h_c}{8k_f} \quad (16)$$

where, $\dot{q} = \mu_{fr} W |V_s|$ is the rate of frictional heat production between the pair of flanks under consideration. The heat partitioning coefficient a_h is calculated as:

$$a_h = \frac{R_{f,g} + R_{c,f}}{R_{f,p} + R_{f,g} + 2R_{c,f}} \quad (17)$$

The thermal resistances of the moving heat source corresponding to the pinion and the gear flank surfaces, $R_{f,p}$ and $R_{f,g}$ as well as the conductive thermal resistance (through the lubricant film) $R_{c,f}$ are calculated as:

$$R_{c,f} = \frac{h_c}{2k_f A_{EHL}} \quad \text{and} \quad R_{c,i} = \frac{1.06}{A_{EHL} k_s} \sqrt{\frac{\chi_{s,i} l_i}{U_{tot,i}}} \quad (18)$$

where, $\chi_{s,i}$ is the thermal diffusivity of surfaces i $(i = p, g)$, whilst l_i is the active length parameter according to Coleman [25]. For the present configuration (hypoid gear pair conjunction) the active length is calculated as:

$$l_i = \sqrt{\frac{{a_c}^2 {b_c}^2 [\tan^2(\theta_i) + 1]}{{a_c}^2 + {b_c}^2 \tan^2(\theta_i)}} \quad (19)$$

where, $\theta_i = \text{atan}(v_i/u_i)$ is the angle between the components of the velocity along the semi-major and the semi-minor axis of the elliptical contact footprint of surfaces i $(i = p, g)$.

2.3-Gear dynamics model

A 4-DoF lumped parameter torsional gear dynamics model is developed (Fig. 4). The torsional compliance of the input and the output shafts (connected at the pinion and the ring gear respectively) is accounted for by substituting them with an equivalent spring/mass/damper element (torsional).

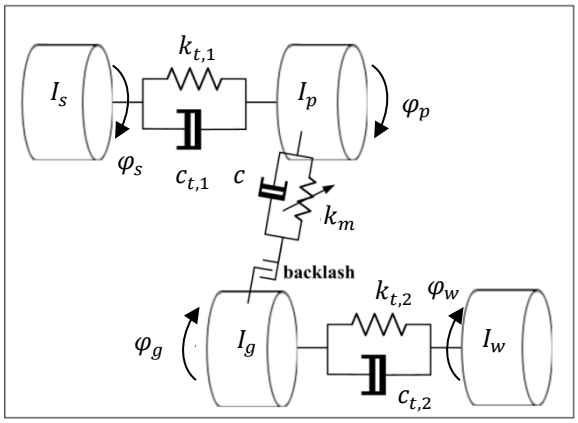

Figure 4: 4-DoF torsional gear dynamics model

The equations of motion are:

$$\ddot{\varphi}_s = \frac{1}{I_s}\left[-k_{t,1}(\varphi_s - \varphi_p) - c_{t,1}(\dot{\varphi}_s - \dot{\varphi}_p) + T_s\right] \quad (20)$$

$$\ddot{\varphi}_p = \frac{1}{I_p}\left[-R_p(k_m f + c\dot{x}) + k_{t,1}(\varphi_s - \varphi_p) + c_{t,1}(\dot{\varphi}_s - \dot{\varphi}_p) + T_{f,p}\right] \quad (21)$$

$$\ddot{\varphi}_g = \frac{1}{I_g}\left[R_g(k_m f + c\dot{x}) - k_{t,2}(\varphi_g - \varphi_w) + c_{t,2}(\dot{\varphi}_g - \dot{\varphi}_w) + T_{f,g}\right] \quad (22)$$

$$\ddot{\varphi}_w = \frac{1}{I_w}\left[k_{t,2}(\varphi_g - \varphi_w) + c_{t,2}(\dot{\varphi}_g - \dot{\varphi}_w) - T_w\right] \quad (23)$$

A constant time step Newmark-beta scheme is employed for the numerical integration of equations (20) – (23). In equations (20) – (23) the backlash function f is calculated according to Kahraman and Singh [26] as:

$$f = \begin{cases} x - b & \text{when} \quad x \geq b \\ 0 & \text{when} \quad -b < x < b \\ x + b & \text{when} \quad x \leq -b \end{cases} \quad (24)$$

The dynamic transmission error (DTE) x is found according to Karagiannis and Theodossiades [27] as:

$$x = \int \left(R_p \dot{\varphi}_p - R_g \dot{\varphi}_g - \dot{e}_0\right) dt \qquad (25)$$

The frictional moments acting on the pinion and the ring gear; $T_{f,p}$ and $T_{f,g}$ are calculated in each time step provided that the magnitude of the flank friction force and its corresponding lever arm to each of the members of the pair is known. The damping coefficients $c_{t,1}$, $c_{t,2}$ and c are calculated through the modal analysis of the linearised system of equations (20) – (23) by assuming $\zeta_1 = 0$ (rigid body mode), $\zeta_2 = 0.02$, $\zeta_3 = 0.04$ and $\zeta_4 = 0.03$. Table 3 lists the gear dynamics related parameters used in the present study.

Table 3: Parameters used in the gear dynamics model

Parameter (unit)	Value
$\boldsymbol{I_s}$ $(\mathbf{kg.m^2})$	1.4×10^{-2}
$\boldsymbol{I_p}$ $(\mathbf{kg.m^2})$	1.4×10^{-2}
$\boldsymbol{I_g}$ $(\mathbf{kg.m^2})$	0.29
$\boldsymbol{I_w}$ $(\mathbf{kg.m^2})$	0.29
$\boldsymbol{k_{t,1}}$ $(\mathbf{Nm/rad})$	8×10^5
$\boldsymbol{k_{t,2}}$ $(\mathbf{Nm/rad})$	8×10^5
$\boldsymbol{b}$ $(\mathbf{m})$	70×10^{-6}

It should be noted that the parameters in table 3 are considered to be common between all the three gear-sets under investigation. This is intentional in order to be able to isolate the effect of contact gear geometry.

Finally, the conjunctional efficiency obtained, corresponds to the RMS of the efficiency variation after 50 meshing cycles under steady state dynamics.

3-Results and Discussion

The results of the tribodynamics analysis for several operating conditions, lubricant formulations and gear-sets are presented. Fig. 5 illustrates a map suggested by Zhang and Gou [28] which can be consulted in order to obtain an estimation of the prevailing regime of lubrication between the mating flanks for a full meshing cycle. The dimensionless groups g_1 and g_2 are calculated according to Zhang and Gou [28], and depend on the operating conditions and the properties of the lubricant used.

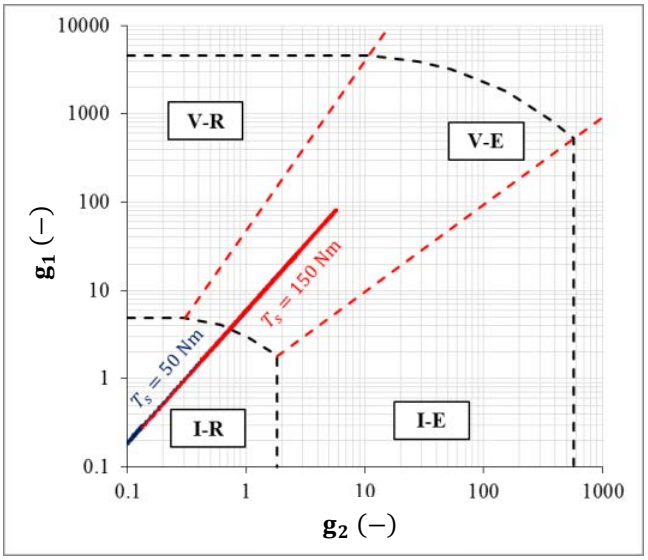

Figure 5: Lubrication regime map (Lubricant OS265962, $T_{bath} = 40$ ℃, $n_p =$ 1000 RPM, gear-set 1)

In Fig. 5, the mode map for 2 complete meshing cycles, each under different operating conditions, has been plotted. The clouds of points (different colour) correspond to different levels of input torque. For both high and low torques, the clouds fall on the same line, although for lower input torques the cloud is shifted towards the lower end of the line, suggesting that a higher number of points within one meshing cycle fall within the iso-viscous rigid (hydrodynamic) regime of lubrication. However, for both cases, the majority of the highly loaded points of the meshing cycle fall within the piezo-viscous elastic (hard EHD) section of the map, indicating that the flank friction force is mainly driven by the mechanisms involved under elastohydrodynamic conditions.

Figure 6a depicts the variation of predicted conjunctional efficiency of gear-set 1 for an increasing pinion speed for the two fluids examined. This shows that the predicted conjunctional efficiency for OS265962 is higher than that for OS265963, although both fluids are of the same viscosity grade (SAE 75W-90). This observation is valid throughout the speed range.

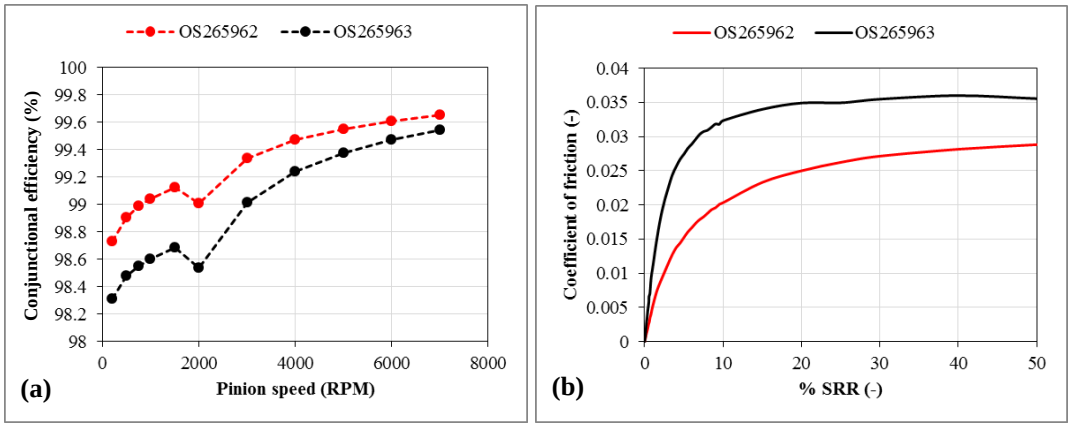

Figure 6: Conjunctional efficiency ($T_s = 100$ Nm (gear-set 1)) (a) and MTM friction (b) ($T_{bath} = 40$ ℃)

The predicted efficiency difference between the 2 fluids under investigation is further supported by the experimentally determined friction curves obtained using a sphere against a flat disk tribometer (i.e. a mini-traction machine; MTM), shown in Fig. 6b. The measured coefficient of friction for OS265963 is considerably larger than that for OS265962 for the entire slide-roll ratios (SRR). This explains the poorer predicted efficiency levels for OS265963, using the tribo-dynamics model, since this is a relatively higher traction fluid. Since both fluids under study are of the same viscosity grade (SAE 75W-90), the key difference between them being responsible for different tractive performance and transmission efficiency, should not be attributed to their viscosity at ambient conditions. It is hypothesised that (1)- high shear and (2)- high pressure piezo-viscous response of these fluids influence their tractive behaviour in hypoid gear pairs. In order to identify which of those two parameters has the greatest contribution, the conjunctional efficiency of OS265963 is predicted using the high pressure viscosity data of OS265962. The results of this analysis is shown in Fig. 7.

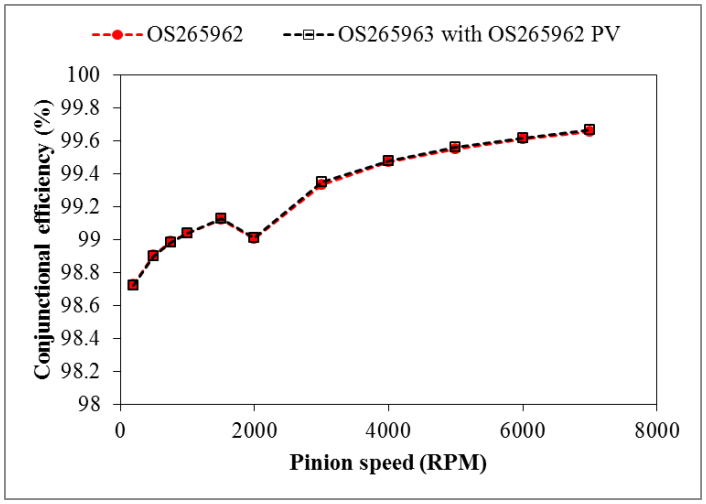

Figure 7: Comparison of the predicted conjunctional efficiency for lubricants OS265962 and OS265963 both having a common high pressure response ($T_{bath} = 40$ ℃, $T_s =$ 100 Nm, gear-set 1)

The results in Fig. 7 suggest that the predicted inefficiency of OS265963 with the high pressure viscosity data of OS265962 is almost identical to the inefficiency predicted for OS265962. Slight deviations are observed at higher pinion speeds which can be attributed to the fact that the shear thinning effect is more prevalent for OS265962 than in OS265963. The almost identical plots in Fig. 7 suggest that high pressure viscosity response of the lubricant, expressed through the PV coefficient (alpha value), is the key influential parameter for conjunctional efficiency. An observation of the lubricant parameters listed in table 2 indicates that the PV coefficient of OS265963 is indeed higher than that of OS265962 throughout the temperature range examined. The higher PV coefficient is responsible for a more dramatic increase in viscosity at the centre (highly pressurised) region of the contact. This yields excessive viscous shear stress, the increase of which does not seem to be compensated by the increase in intensity shear heating of the fluid, hence the increase in the frictional power losses. The different PV responses of the fluids can be attributed to the different type and concentration of the VM blended in each case.

Further to the contribution of the lubricant formulation, the plots in Fig. 6a indicate a sudden decrease in conjunctional efficiency when the pinion speed reaches 2000 RPM. As shown in Fig. 8, this behaviour is amplified for a decreased input torque (50 Nm), whilst it ceases for higher torque levels (200 Nm, 300 Nm).

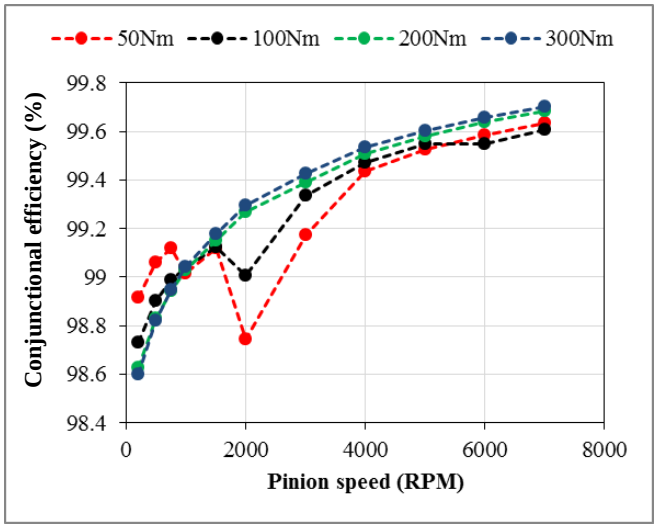

Figure 8: Variation of the conjunctional efficiency with the pinion speed at various input torques for lubricant OS265962 at $T_{bath} = 40$ ℃ (gear-set 1)

An explanation for this behaviour can be found in the dynamic response of the system, and particularly the appearance of resonance. Fig. 9 shows that for 100 Nm peak-to-peak response of the DTE at 2000 RPM the characteristic jump phenomenon occurs, heralding the emergence of resonant conditions [29]. Furthermore, for the same operating conditions, the minimum amplitude of the DTE falls below the half backlash line, indicating that single sided tooth impacts would occur, meaning that for a certain period of time within the meshing cycle, the mating teeth lose contact. Other studies have shown that contact separation occurs with lack of friction, leading to noise and vibration phenomenon such as axle whine in vehicle differential systems [30]. Friction is the main source of system damping as it acts as an energy sink. The other source, squeeze film lubrication has shown to be minimal under elastohydrodynamic regime of lubrication [31, 32].

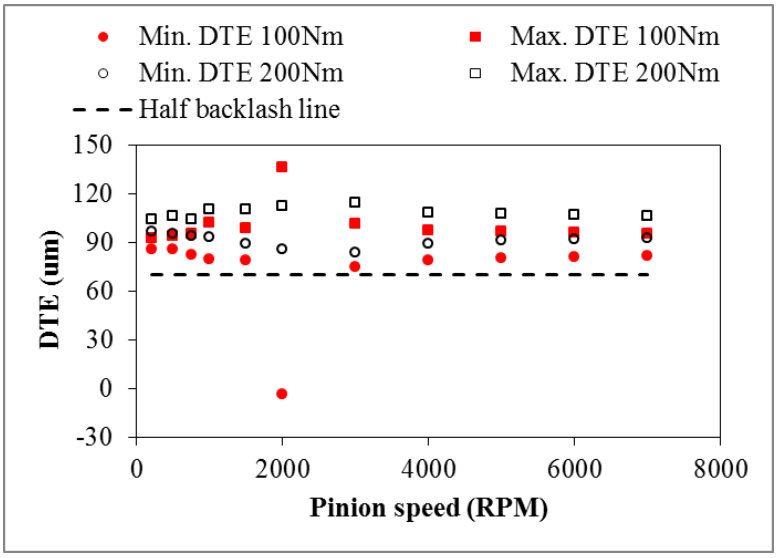

Figure 9: Peak response of the DTE (Lubricant OS265962 at $T_{bath} = 40$ ℃, gear-set 1)

The decreased conjunctional efficiency during resonance can be explained by the plots in Fig. 10a-b, where the variation of flank contact load within one engagement cycle is plotted for two different input speeds, 2000 RPM (close to resonance) and 5000 RPM (away from resonance). During the onset of engagement at 2000 RPM the contact load appears to diminish, corresponding to teeth pair separation. Despite the fact that the gear pair operates under the same torque level for both speeds (2000 RPM and 5000 RPM), the average contact load appears is higher for 2000 RPM (resonance) (Fig. 10a). At the same time, the average coefficient of friction for 2000 RPM is also higher than that for 5000 RPM (Fig. 10b) which accounts for reduced efficiency at lower speeds. Furthermore, the loss of friction (coefficient of friction of zero in Fig. 10b) indicates no instantaneous friction, thus the resonant conditions and the occurrence of jump phenomenon.

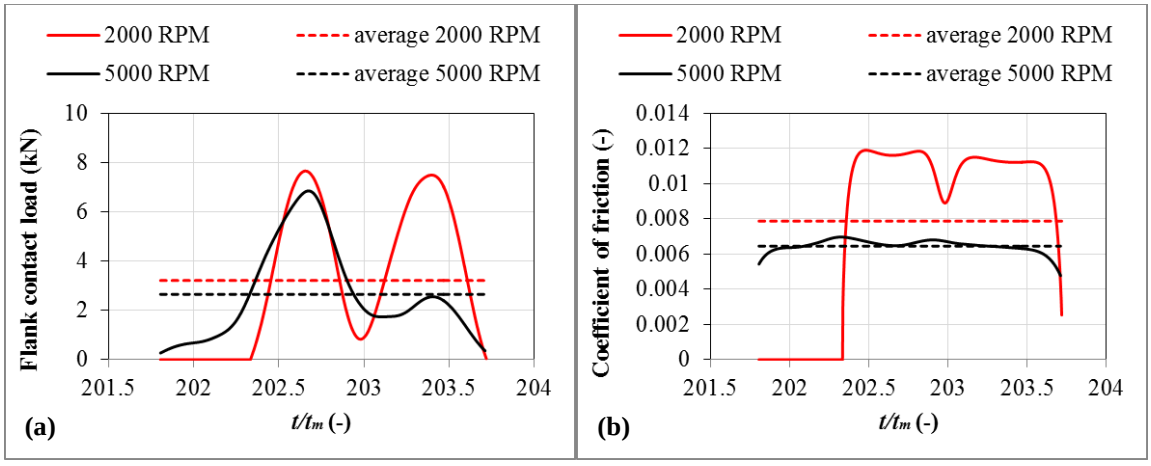

Figure 10: Flank contact load (a) and flank coefficient of friction (b) (Lubricant OS265962 at $T_{bath} = 40$ ℃, gear-set 1)

Finally, Fig. 11 compares the predicted conjunctional efficiency between gear-set 2 (2.73 gear ratio) and gear-set 3 (3.41 gear ratio). A non-uniform variation in conjunctional efficiency of gear set 2 is observed for pinion speeds ranging from 1000 RPM to 2000 RPM. Again, these irregularities are attributed to the appearance of resonance, which is illustrated by the plots of Fig. 11b. For this range of pinion speeds, gear-set 2 experiences high DTE amplitudes, due to resonance with super-harmonic responses, while the DTE amplitude for gear-set 3 is reduced. This discrepancy is due to the different meshing stiffness characteristics of each gear-set, since their inertial properties are assumed to be the same.

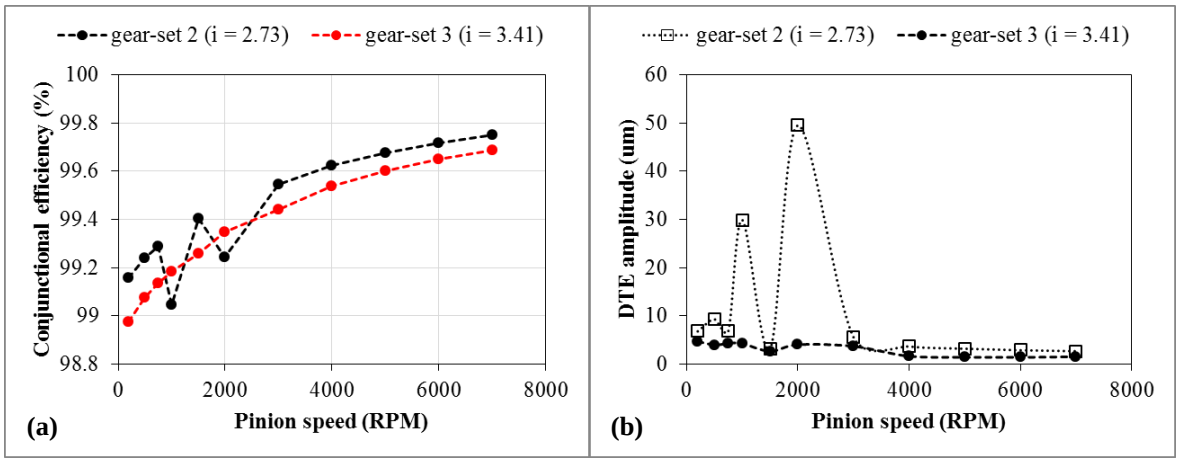

Figure 11: Conjunctional efficiency (a) and DTE amplitude (b) ($T_{bath} = 40$ ℃, $T_s =$ 100 Nm, lubricant OS265962, gear-sets 2 and 3)

Fig. 11a shows improved efficiency for gear-set 2 relative 2 gear-set 3, at least for operating conditions away from resonance. This discrepancy can be explained by the increased contact load supported by gear-set 2 since the input torque is the same for both the plots as shown in figures 11a,b.

4-Conclusions

A hypoid gear pair tribodynamic model is presented. Particular attention is paid to the influence of lubricant formulation, the dynamic response of the system and the gear pair geometry upon the resulting conjunctional efficiency. The main findings of the study are:

- The qualitative trends of simple laboratory measurements (MTM) can be potentially used as an indication of the relative efficiency performance of the lubricants

considered when these are used in a full scale system (such as the hypoid gear pair unit).

- Gear lubricants of the same viscosity grade can potentially exhibit different conjunctional efficiency responses.
- Different types and concentrations of VM in the same fluid can result in different conjunctional efficiency.
- The high pressure viscosity response of the lubricant is the key parameter affecting transmission efficiency.
- The appearance of resonance (torsional mode) deteriorates the conjunctional efficiency and is primarily cause by loss of contact and diminished friction, exhibited by the jump phenomenon.
- For the same input torque, hypoid gear pairs of lower gear ratio exhibit improved conjunctional efficiency. This is due to the reduced contact load supported by the mating flanks for a given input torque.

Acknowledgments

The authors would like to express their gratitude to Lubrizol Ltd. for the financial support of this research. Thanks are due to Dr. Farrukh Qureshi (Lubrizol Corporation, Wickliffe, OH, USA) for the provision of high pressure viscometry, Dr. Eugene Pashkovski (Lubrizol Corporation, Wickliffe, OH, USA) for high shear viscosity data and to Dr. Sandeep Vijayakar from Advanced Numerical Solutions (ANSOL) (Hilliard, OH, USA) for his kind permission to use the TCA software CALYX. Finally, the authors would like to thank Dr. Mohsen Kolivand of American Axle (Detroit, MI, USA) for providing valuable input with regards to gear geometry.

Nomenclature

a_c semi-major axis half-width (m)

A_{asp} area of asperity contact (m^2)

A_{EHL} total area of elliptical contact footprint (m^2)

a_h heat partitioning coefficient ($-$)

b half backlash length (m)

b_c semi-minor axis half-width (m)

$[C]$ damping matrix of the linearised dynamical system $(\mathrm{Nm.s/rad})$

c mesh damping coefficient $(\mathrm{Ns/m})$

$c_{p,f}$ heat capacity of the lubricant $(\mathrm{J/kg.K})$

$c_{t,i}$ torsional damping coefficient of the i^{th} $(i = 1,2)$ shaft $(\mathrm{Nm.s/rad})$

E Young's modulus of elasticity of the gear material (steel) (Pa)

E^* reduced Young's modulus of elasticity of the mating teeth $(E^* = E/(1-\nu^2))$ (Pa)

e_0 unloaded static transmission error (m)

F shear thinning function of the lubricant $(-)$

F_b flank boundary friction (N)

F_{fr} flank total friction (N)

F_v flank viscous friction (N)

f backlash function (m)

F_2 a statistical function

$F_{5/2}$ a statistical function

G dimensionless material's parameter $(-)$

g_1 mode of lubrication dimensionless parameter

g_2 mode of lubrication dimensionless parameter

h_c central lubricant film thickness (m)

I_i mass moment of inertia of the i^{th} $(i = s, p, g, w)$ of the dynamical system $(\mathrm{kg.m^2})$

$[K]$ stiffness matrix of the linearised dynamical system $(\mathrm{Nm/rad})$

k_f thermal conductivity of the lubricant $(\mathrm{W/m.K})$

k_m meshing stiffness of the gear pair $(\mathrm{N/m})$

k_s thermal conductivity of the material of the gear teeth (steel, $k_s = 30$ $\mathrm{W/m.K}$) $(\mathrm{W/m.K})$

$k_{t,i}$ torsional stiffness of the i^{th} $(i = 1,2)$ shaft $(\mathrm{Nm/rad})$

l_i thermal active length of the i^{th} $(i = p, g)$ flank in the conjunction (m)

lf_k load sharing factor of the k^{th} $(k = 2 \div 3)$ pair of flanks $(-)$

$[M]$ mass matrix of the linearised dynamical system $(\mathrm{kg.m^2})$

N_p number of teeth of the pinion $(-)$

n_p speed of the pinion (RPM)

p pressure of the lubricant (Pa)

$\dot{q}$ frictional heat production rate between a pair of flanks (W)

$R_{c,f}$ conductive thermal resistance through the lubricant film (K/W)

R_e effective contact radius of curvature along the direction of entraining motion (m)

$R_{f,i}$ conductive thermal resistance for the moving heat source on the i^{th} $(i = p, g)$ flank surface (K/W)

R_p contact radius of the pinion (m)

R_s effective contact radius of curvature along the side leakage direction (m)

t time (s)

T_{bath} bulk temperature of the lubricant in the lubricant bath (℃, K)

$\overline{T}_c$ average temperature of the lubricant at the centre of the EHD conjunction (℃, K)

$T_{f,i}$ total frictional torque acting on the i^{th} $(i = p, g)$ member of the gear pair (Nm)

T_{in} inlet temperature of the lubricant in the EHD conjunction (℃, K)

T_s torque applied on the pinion shaft (Nm)

T_w torque applied on the gear shaft (Nm)

U_e dimensionless speed parameter or rolling viscosity parameter $(-)$

u_i surface velocity of the i^{th} $(i = p, g)$ flank along the semi-minor axis of the contact ellipse (m/s)

$U_{tot,i}$ total surface velocity of the i^{th} $(i = p, g)$ flank (m/s)

v_i surface velocity of the i^{th} $(i = p, g)$ flank along the semi-major axis of the contact ellipse (m/s)

V_s total sliding velocity between the mating flanks of the flank pair under consideration (m/s)

W_{asp} load carried by the asperities (N)

W_e dimensionless load parameter $(-)$

W_k load carried by the k^{th} $(k = 2 \div 3)$ pair of flanks (N)

W_t total contact load (N)

x dynamic transmission error (m)

Greek symbols

α^* reciprocal asymptotic iso-viscous pressure viscosity coefficient (Pa^{-1})

α_{HN} Havriliak – Negami exponent $(-)$

β_{HN}	Havriliak – Negami exponent $(-)$
β_s	average radius of curvature of the tips of the asperities (m)
$\dot{\gamma}$	lubricant film shear rate (s^{-1})
$\left(\Delta T_f\right)_{av}$	average temperature rise of the lubricant (K)
$(\Delta T_{oil})_{av}$	average temperature rise of the lubricant due to shear heating (K)
ζ_i	damping ratio of the i^{th} $(i = 1,2,3,4)$ mode shape of the linearised dynamical system $(-)$
η	dynamic viscosity of the lubricant $(\mathrm{Pa.\,s})$
η_s	asperity peak density per unit area of surface $(1/\mathrm{m}^2)$
θ_i	angle between the components of the surface velocity of the i^{th} $(i = p, g)$ flank (rad)
λ	lubricant relaxation time (s)
λ_s	Stribeck's lubricant film parameter for flank pairs $(-)$
ν	Poisson's ratio of the gear material (steel) $(-)$
σ_s	RMS surface height of the asperity tips on the pinion flank (m)
$\sigma_{s,c}$	combined RMS surface height of the asperity tips between the mating flanks (m)
ς_a	Shear strength coefficient of asperity pairs $(-)$
$\overline{\tau}$	average conjunctional shear stress (Pa)
τ_0	Eyring shear stress (Pa)
φ_i	rotation angle of the i^{th} $(i = s, p, g, w)$ member of the dynamical system (rad)
$\chi_{s,i}$	thermal diffusivity of the gear material (steel) $(\mathrm{m}^2/\mathrm{s})$
ω_m	meshing angular frequency of the gear pair $(\mathrm{rad/s})$
ω_p	angular velocity of the pinion $(\mathrm{rad/s})$

References

[1]- Mohammadpour, M., Theodossiades, S. and Rahnejat, H., "Elastohydrodynamic lubrication of hypoid gear pairs at high loads", Proc. IMechE, Part J: J. Engineering Tribology, 2012, 226(3), pp. 183-198.

[2]- Paouris, L., Theodossiades, S., De la Cruz, M., Rahnejat, H., Kidson, A., Hunt, G. and Barton, W., "Lubrication analysis and sub-surface stress field of an automotive differential

hypoid gear pair under dynamic loading", Proc. IMechE, Part C: J. Mechanical Engineering Science, 2016, 230(7-8), pp. 1183-1197.

[3]- Kubo, K., Shimakawa, Y. and Kibukawa, M., "The effect of gear oil viscosity and friction reducer type on transmission efficiency", Tribol. Int., 1986, 19, pp. 312–317.

[4]- Xu, H. and Kahraman, A., "Prediction of friction-related power losses of hypoid gear pairs", Proc. IMechE, Part K: J. Multi-Body Dyn., 2007, 221, pp. 387–400.

[5]- Karagiannis, I., Theodossiades, S. and Rahnejat, H., "On the dynamics of lubricated hypoid gears", Mech. Mach. Theory, 2012, 48, pp. 94–120.

[6]- Mohammadpour, M., Theodossiades, S., Rahnejat, H. and Kelly P., "Transmission efficiency and noise, vibration and harshness refinement of differential hypoid gear pairs", Proc. IMechE, Part K: J. Multi-Body Dyn., 2014, 228(1), pp. 19-33.

[7]- Mohammadpour, M., Theodossiades, S. and Rahnejat, H., "Transient mixed non-Newtonian thermo-elastohydrodynamics of vehicle differential hypoid gears with starved partial counter-flow inlet boundary", Proc. IMechE, Part J: J. Engineering Tribology, 2014, 228(10), pp.1159-1173.

[8]- Talbot, D., Kahraman, A., Li, S., Singh, A. and Xu, H., "Development and validation of an automotive axle power loss model", Tribol. Trans., 2016, DOI:10.1080/10402004.2015.1110862

[9]- Vijayakar, S. M., "Tooth contact analysis software Calyx", Advanced Numerical Solutions, Hilliard, OH, USA, 1998.

[10]- Karagiannis, I., Theodossiades, S. and Rahnejat, H., "The effect of vehicle cruising speed on the dynamics of automotive hypoid gears", SAE Tech., Pap. No. 2012-01-1543, 2012.

[11]- Wang, Y., Lim, T. C. and Yang, J., "Multi-point mesh modelling and nonlinear multi-body dynamics of hypoid geared system", SAE Int. J. Passenger Cars-Mechanical Systems, 6(2013-01-1895), 2013, pp.1127-1132.

[12]- Hamrock, B. and Dowson, D., "Ball bearing lubrication – the elastohydrodynamics of elliptical contacts", John Willey and Sons, 1981.

[13]- Roelands, C., "Correlational aspects of the viscosity-temperature pressure relationship of lubricating oils", PhD Thesis, Delft Technical University, 1966.

[14]- Vogel, H., "The law of the relation between the viscosity of liquids and the temperature", Phys. Z., 1921, 22, pp. 645-646.

[15]- Havriliak, S. and Negami, S., "A complex plane representation of dielectric and mechanical relaxation processes in some polymers", Polymer (Guildf), 1967, 8, pp. 161–210.

[16]- Chittenden, R. J., Dowson, D., Dunn, J. F. and Taylor, C. M., "A theoretical analysis of the isothermal elastohydrodynamic lubrication of concentrated contacts. II. General case, with lubricant entrainment along either principal axis of the Hertzian contact ellipse or at some intermediate angle", Proc. Roy. Soc., Ser. A: Math. Phys. Eng. Sci., 1985, 397, pp. 271–294.

[17]- Teodorescu, M., Balakrishnan, S. and Rahnejat, H., "Integrated tribological analysis within a multi-physics approach to system dynamics", Tribology and interface Engineering Series, 2005, 48, pp. 725-737.

[18]- Briscoe, B. J. and Evans, D. C. B., "The shear properties of Langmuir-Blodgett layers", Proc. Roy. Soc. London, 1982, 380, pp. 389–407.

[19]- Styles, G., Rahmani, R., Rahnejat, H. and Fitzsimons, B., "In-cycle and life-time friction transience in piston ring–liner conjunction under mixed regime of lubrication", Int. J. Engine Research, 2014, 15(7), pp. 862-876.

[20]- Leighton, M., Rahmani, R. and Rahnejat, H., "Surface-specific flow factors for prediction of friction of cross-hatched surfaces", Surface Topography: Metrology and Properties, 2016, 4(2):025002.

[21]- Greenwood, J. A. and Tripp, J. H., "The contact of two nominally flat rough surfaces", Proc. Inst. Mech. Eng., 1970-1971, 185, pp. 625–633.

[22]- Gohar, R. and Rahnejat, H., "Fundamentals of Tribology", Imperial College Press, London, 2008.

[23]- Olver, A. V., "Gear lubrication - a review", Proc. IMechE, Part J: J. Eng. Tribol., 2002, 216, pp. 255–267.

[24]- Olver, A. V., "Testing transmission lubricants: the importance of thermal response",

Proc. IMechE, Part G: J. Aerosp. Eng., 1991, 205, pp. 35–44.

[25]- Coleman, W., "A scoring formula for bevel and hypoid gear teeth", J. Tribol., 1967, 89, pp. 114–123.

[26]- Kahraman, A. and Singh, R., "Non-linear dynamics of a spur gear pair", J. Sound and Vib., 1990, 142, pp. 49–75.

[27]- Karagiannis, I. and Theodossiades, S., "An alternative formulation of the dynamic transmission error to study the oscillations of automotive hypoid gears", J. Vib. and Acoust., 2013, 136, pp. 1–12.

[28]- Zhang, P. S. and Gou, J. H., "Two new formulae to calculate the film thickness in elastohydrodynamic lubrication and an evaluation of Grubin's formula", Wear, 1989, 130, pp. 357–366.

[29]- Ozguven, H. N. and Houser, D. R., "Dynamic analysis of high speed gears by using loaded static transmission error", J. Sound and Vib., 1988, 125, pp. 71–83.

[30]- Koronias, G., Theodossiades, S., Rahnejat, H. and Saunders, T., "Axle whine phenomenon in light trucks: a combined numerical and experimental investigation", Proc. IMechE, Part D: J. Automobile Eng., 2011, 225(7), pp. 885-894.

[31]- Dareing, D.W. and Johnson, K.L., "Fluid film damping of rolling contact vibrations", J. Mech. Eng. Sci,, 1975, 17(4), pp. 214-218.

[32]- Mehdigoli, H., Rahnejat, H. and Gohar, R., "Vibration response of wavy surfaced disc in elastohydrodynamic rolling contact", Wear, 1990, 139(1), pp. 1-5.